Industrial Health 2010, **48**, 43–51 **Original Article**

Significance of Face Velocity Fluctuation in Relation to Laboratory Fume Hood Performance

Li-Ching TSENG[1], Rong Fung HUANG[2]* and Chih-Chieh CHEN[3]

[1]Department of Safety and Health, Council of Labor Affairs, 83 Yanping N. Road, Section 2, Taipei, Taiwan
[2]Department of Mechanical Engineering, National Taiwan University of Science and Technology, 43 Keelung Road, Section 4, Taipei, Taiwan
[3]Institute of Occupational Medicine and Industrial Hygiene, National Taiwan University, 1 Jen-Ai Rd., Sec. 1, Taipei, Taiwan

Received November 4, 2008 and accepted July 1, 2009

Abstract: In order to recognize the problems associated with the transport mechanism of containment during the ventilation process of a laboratory fume hood, a transparent, full scale chemical fume hood is constructed for experimental studies. Distributions of mean velocity and velocity fluctuation in the sash plane are measured using a thermal anemometer. Flow patterns and tracer-gas concentration leakages are respectively diagnosed via the laser-assisted flow visualization method and the EN 14175-3 test protocol. The magnitudes of measured velocity fluctuations exhibit a sharp peak along the perimeter of the sash opening. The results of flow visualization verify that the elevated turbulence fluctuations are induced by the boundary-layer separation when the flow passes over the edges of sash perimeter. The tracer gas experiment shows that the regions where high degree containment leakages detected are located along the perimeter of hood aperture. Eleven commercial hoods which are claimed with fine aerodynamic design are further tested for confirmation of these observations. The results show similar correlations. Conclusions thus are made that large-scale vortex structures occurring around the perimeters of hood aperture due to the boundary-layer separation could induce strong turbulence, and therefore enhance dispersion of the hood containment.

Key words: Laboratory fume hood, Tracer gas test, Flow visualization, Turbulence

Introduction

A laboratory fume hood is designed to capture, contain and remove harmful fumes generated inside the box-like enclosure. The performance and characteristics of laboratory fume hoods have been widely studied during the past few decades. Previous studies[1–7] suggested that maintaining a specific face velocity does not assure that a fume hood would contain hazardous chemical fumes and vapors. Important parameters, such as fume hood geometry, suction flow rates, sampling rates and sash opening height, etc., affect the containment ability of laboratory fume hoods. Although average face velocity and containment efficiency are related under ideal conditions, it is very difficult in nature to use only a parameter, the face velocity, to characterize the hood performance.

Durst *et al*.[8, 9] employed numerical predictions of the aerodynamic flow field inside two-dimensional fume hood with baffles. Several flow configurations were predicted and particular attention was devoted to the ambient flow entrainment into the fume hood for different sash heights and different conditions of the exhaust system. Hu *et al*.[10, 11] presented the flow in the region of a fume hood using the turbulent model and CFD (computational fluid dynamics). The potential of various factors that cause the leakage of contaminant from the fume hood were investigated, in particular the effect of the location of the exhaust outlet, exterior obstructions of different shapes and sizes in front of the fume hoods, baffles and a louvered bypass. The air velocity and concentration of contaminant profiles along the working aperture were

*To whom correspondence should be addressed.
E-mail: rfhuang@mail.ntust.edu.tw

obtained using the numerical predictions and compared with experimental data. Nicholson *et al*.[12] demonstrated that the potential of using CFD model for the optimization of fume hood design and testing. Lan *et al*.[13] and Kirkpatrick *et al*.[14] employed three-dimensional models of a variable volume/constant face velocity fume hood to study the effect of the sash height and rated face velocity on the flow patterns, especially in the exposure area of a person standing in front of the fume hood.

In this study, detailed experimental data on this subject and the extent of the understanding on the physical mechanisms governing the leakage of contaminant during the ventilation process are investigated. Measurements of the time-averaged face velocity, velocity fluctuation profiles, and real-time tracer-gas concentration leakage along the face of the hood were conducted. The laser-light sheet smoked-flow visualization method was incorporated in providing details of the aerodynamics at the face of the fume hood and served to explain the transport mechanism of contaminant leakage near the face of the hood.

Materials and Methods

Laboratory test apparatus

The experimental setup includes a laboratory fume hood model, an extract fan, and instruments as shown in Fig. 1. The test fume hood with 850 mm × 1,200 mm in size of working aperture is made of transparent acrylic plates so that the laser beams can pass through. The fume hood consists of a baffle across its back. The baffle has a top slot and a bottom slot to help effectively remove the contaminant through the fume hood. The top panel of the hood has an exhaust collar to connect the exhaust duct to the fume hood. Suction of the hood is provided via a set of AC motor/centrifugal fan. The suction flow is driven by a centrifugal fan which is controlled by a precision inverter with a resolution of 0.02 Hz. The suction flow rate is measured by a home-made venturi flow meter along with a calibrated pressure gauge. Long term monitoring of the flow rate measurements shows no appreciable drifts or ripples. The accuracy of the suction flow rate measurement is less than 1% of the reading. Experiments are carried out in a well-controlled test room. The test room consists of an enclosure with dimensions of 19.14 m × 16.53 m × 4.76 m. During the experiment, the turbulence and interference from external sources such as air supply diffusers, doors, and traffic in the room are restricted.

Flow visualization

The experimental apparatus for flow visualization is shown in Fig. 2. Paraffin oil mist was continuously seeded through the home-made smoke generator into the test section to scatter the laser light. The diameter of the oil-mist particles, measured by a Malvern 2600C particle analyzer, is 1.7 ± 0.2 μm. The density of this particle is 0.821 g/ml. Without considering the effect of turbulent diffusion, the relaxation time constant is estimated to be less than 7.7×10^{-5} s and the Stokes number is in the order of 10^{-6} within the range of experiment. Therefore, the seeding particles can properly follow the flow fluctuations at least up to 10 kHz.

The streams of the visible smoke were discharged by two different means. First, for simulating the contami-

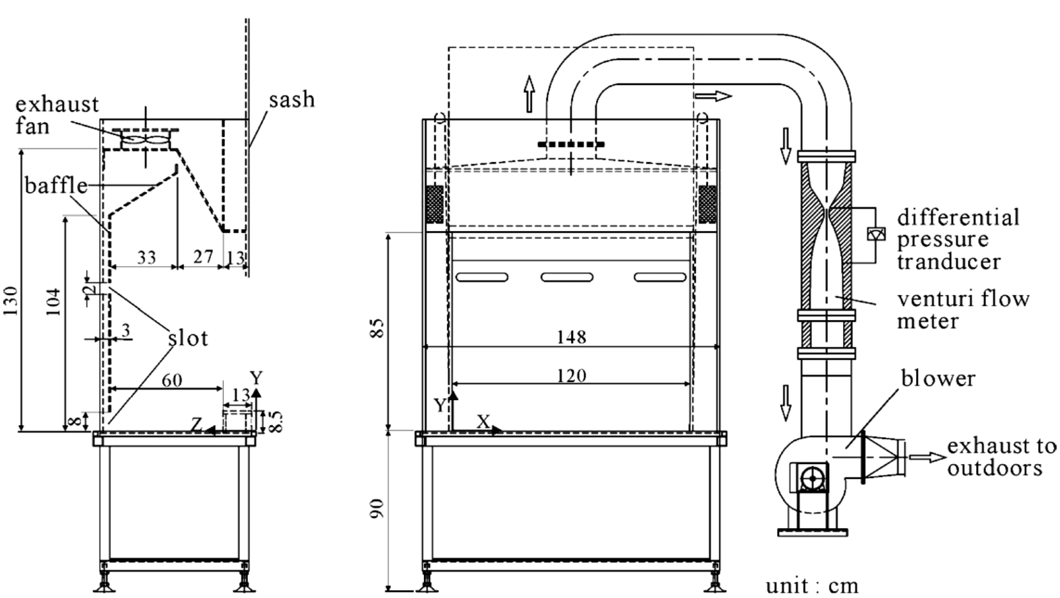

Fig. 1. Experimental setup.

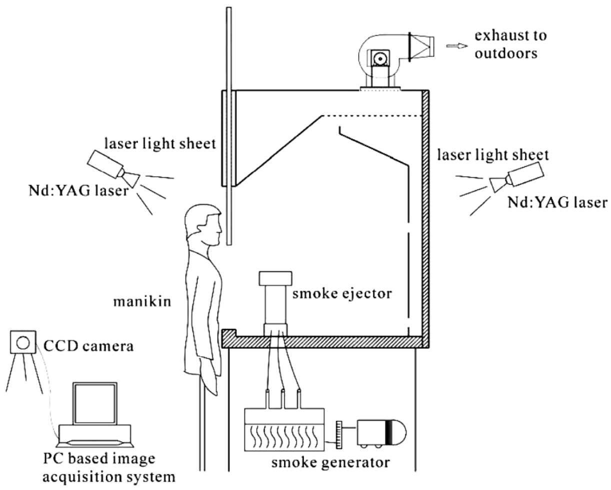

Fig. 2. Experimental apparatus for flow visualization.

nant transport process, the smoke was generated from the smoke generator and piped to the smoke ejector. Second, for better visualization of the flow structure in the test section in corresponding to the contaminant transport behavior, the ejector tubes were positioned at target test sections for releasing a uniform outlet velocity of smoke. The smoke generator used in this experiment was equipped with six tubes, and each tube was connected to a ball valve. The smoke ejector was made of stainless still and was installed at center position that is equidistant from the inside wall of the hood, and the position was with the front of the ejector body 150 mm form the hood face. The smoke was distributed through a wire mesh outlet diffuser with a smoke release rate of 4 l/min. The laser beam from Nd:YAG laser was transmitted through an optical fiber and connected to a 20° laser-light sheet expander. The laser-light sheet expander was mounted on an adjustable block so that the light sheet can be aligned on different planes. The laser-light sheet was adjusted to a thickness of about 0.5 mm. The particle images were recorded by a Hi-8 CCD camera. The camera was equipped with an asynchronous variable electronic shutter, ranging from 1/12,000 to 1/30 s and could record images at 30 fps.

Face velocity and fluctuation measurements

Two suction rates $Q = 0.51$ m^3/s and 0.31 m^3/s are used for tests. The maximum sash height H_0 is 85 cm. Measurements of time-averaged face velocity and velocity fluctuations are conducted at four different sash heights: H/H_0 = 100%, 75%, 50%, and 25%. The face velocities V_0 correspond to these sash heights are (0.5, 0.67, 1.0, 2.0) m/s for Q = 0.51 m^3/s and (0.3, 0.4, 0.6, 1.2) m/s for Q = 0.31 m^3/s. The rectangular area of the sash plane is defined by the vertical and horizontal boundaries. Four equally spaced lines between the vertical side-boundaries of the sash plane are divided into four vertical heights of Y/H = 0.875, 0.625, 0.375, and 0.125 at each sash height. Fifteen equally spaced lines between the horizontal side-boundaries of the sash plane are set and the lines in between are at a distance of 80 mm. The anemometer probe is positioned at each of the center of the grid formed by the intersection of the above vertical and horizontal lines of the sash plane. Face velocities are measured at 60 points across the sash plane using a thermal anemometer (Alnor Model 8565 Thermoanemometer, Alnor Instrument Co., Skokie, Illinois). The anemometer is calibrated in a wind tunnel periodically throughout the study. The sample rate is 200 data/s, and the elapse time is 180 s. The accuracy is ± 1.5% of the reading. The time-averaged face velocities, V, and the velocity fluctuations, V_{std}, at each spatial point are calculated based on the measured "instantaneous" velocity data V_i by using the following equations (1) and (2), respectively.

$$V = (\frac{1}{N})\sum_{i=1}^{N} V_i \tag{1}$$

$$V_{std} = [(\frac{1}{N-1})\sum_{i=1}^{N}(V_i - V)^2]^{1/2} \tag{2}$$

Equation (1) represents the arithmetic average of velocity over the sampled N instantaneous velocity data. The eqn. (2) is the standard deviation of velocity data, which is actually the root-mean-square value of the fluctuating velocities would give a representation of the statistical value of the velocity fluctuations[15] about the average velocity over the measurement time at each grid position. The standard deviation normalized by the average velocity would therefore represent the turbulence intensity[15].

Static tracer gas test following EN 14175-3 Protocol

The measurements were conducted in accordance with the EN 14175-3 protocol[16] by using 10% SF_6 in N_2 as the tracer gas. The tracer gas ejector was a hollow cylinder made of sintered metal with a length 25 mm and a diameter 15 mm in accordance with this method. The release rate of the tracer gas was 2.0 l/min. As shown in Fig. 3, nine sampling probes were arranged in a grid based on a square area of 200 mm × 200 mm. There were three vertical and three horizontal grid lines separated from each other by 100 mm in both directions. The tracer gas ejector was arranged with its center in-line and 150 mm from the center of the sampling probe grid. The axis of the central probe in the grid was in line with the mid-point of the ejector. The central sampling probe grids were positioned on the sash plane with its center probe at points formed by the intersection of three equally

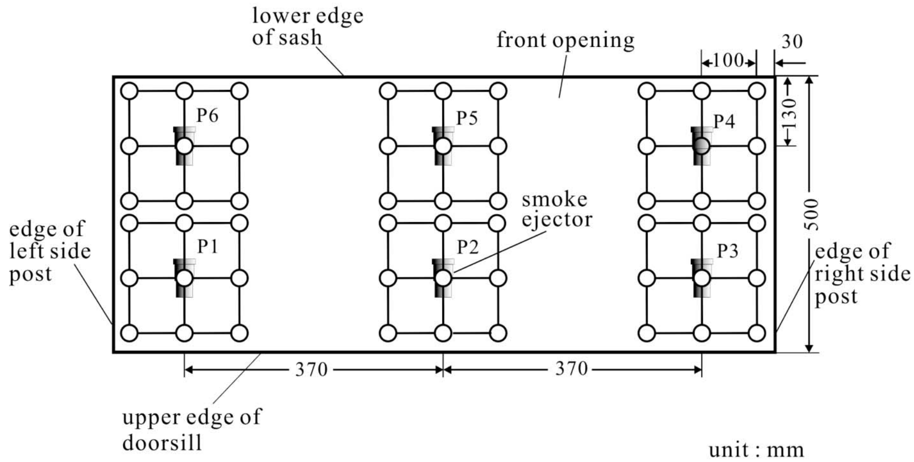

Fig. 3. Sampling grid and source position arrangements by employing dynamic containment test of EN 14175 method.

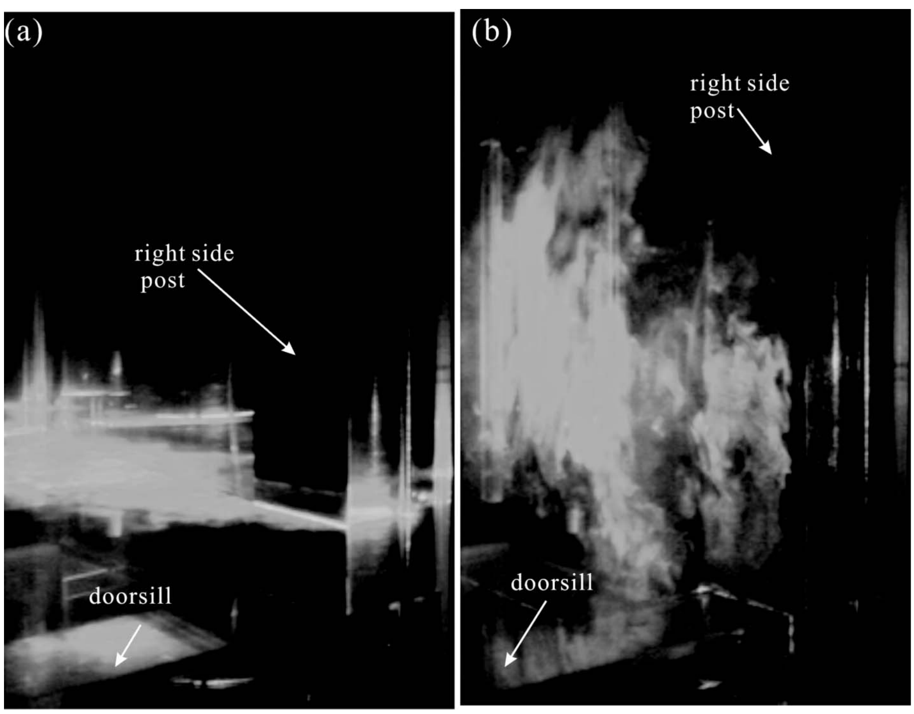

Fig. 4. Smoke flow patterns near right side post. H = 50 cm, V_0 = 0.5 m/s. (a) horizontal view, (b) vertical view.

spaced lines between the horizontal boundaries of the sash plane with the two outermost lines 130 mm from the horizontal boundaries. The sampling probes were connected to the sampling manifold by tubes of equal lengths. The detector probe was affixed to the output of the manifold. Tracer gas samples were taken through a stainless steel tube of 8 mm internal diameter, which was fitted with a diffuser of 30 mm internal diameter at inlet end of suction velocity 3.7 cm/s. Sampling was taken for 360 s.

Results and Discussion

Flow visualization

Figures 4(a) and 4(b) show respectively the horizontal and vertical views of smoke flow patterns near the right post. The smoke particles are released via a smoke ejector which is placed on the work surface. Because of the three-dimensional flow structure generated in the hood, the smoke particles are brought to the side wall regions. It can be seen that when the environmental air is drawn

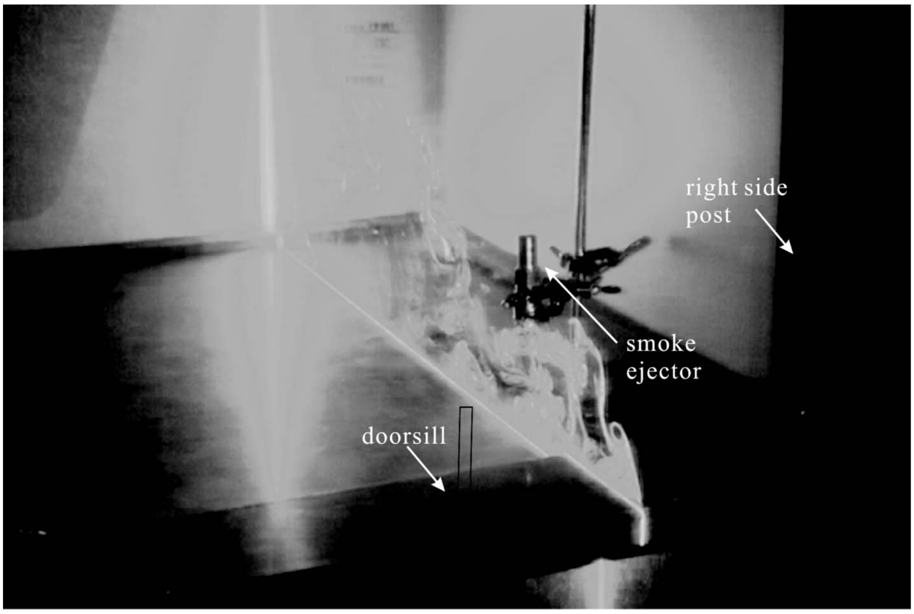

Fig. 5. Horizontal view of smoke flow patterns near doorsill. H = 50 cm, V_0 = 0.5 m/s.

into the hood and past the post, a severe boundary-layer separation occurs. The boundary layer separates from the edge of the post and forms a shear layer with coherent structures. The separated shear layer inherently contains large turbulence fluctuations from the point of view of fluid mechanics[17]. The separated boundary layer evolves into the hood and forms a large recirculation bubble near the side wall. The containments in the hood would be entrained by the recirculating current and carried towards the separated shear layer. Turbulent dispersion across the shear layer may happen due to the high turbulence fluctuation property of the shear layer. It is therefore possible that the containments in the hood diffuse through this area.

Figure 5 shows the vertical view of smoke flow pattern near the doorsill. The smoke particles are released via a smoke ejector placed inside the hood, 15 cm away from the doorsill. It can be seen that when the environmental air is drawn into the hood and past the doorsill, the boundary layer separates from the front edge of the doorsill. The separated shear layer contains coherent structures. Similar to the phenomenon occurs near the side posts, turbulent dispersion across the separated boundary layer may happen due to high turbulence fluctuation property of the shear layer. This area therefore would possibly subject to leakage of containment.

Mean face velocity and velocity fluctuation

Measurements of the time-averaged face velocity and velocity fluctuation are conducted on the sash plane at four different sash heights. The results are shown in Figs. 6 and 7 for the suction rates Q = 0.51 and 0.31 m^3/s, respectively. The features of the velocity and fluctuation distributions at the high (Q = 0.51 m^3/s) and low (Q = 0.31 m^3/s) flow rates are quite similar because they are all subjected to the influence of boundary-layer separations along the peripheral of the aperture and are all in the turbulence regime in the sense of fluid mechanics. They are therefore discussed together as follows. It can be seen that the dimensionless mean velocity distributions (V/V_0) across X at four vertical height Y positions have different shapes with various magnitudes at both suction rates. The mean velocity distributions consist of a relatively uniform regime around the core region of the sash opening and a shear regime near the side posts and doorsill. Each of the horizontal profiles of V/V_0 for Y/H = 0.875, 0.625, 0.375 and 0.125 declines to the lowest values near the right and left side posts of the hood at either Q = 0.51 or 0.31 m^3/s. At the lowest vertical height Y/H = 0.125, i.e. near the doorsill face of the hood, the magnitudes of the mean face velocity present much lower values than those measured at the upper grids. The mean velocities near the side posts and doorsill are sharply decreased because of the "no-slip condition" induced by the fluid viscosity at the walls[17].

The standard deviation of the measured velocities, V_{std}, can be taken as an index for the intensity of velocity fluctuation. The dimensionless velocity fluctuations, i.e. V_{std}/V_0, near the right and left side posts are significantly higher than those at other grids of the same heights. Besides, at the lowest vertical height of Y/H = 0.125, i.e. near the doorsill of the hood, the velocity fluctuations attain significantly higher levels than the corresponding upper grids at either Q = 0.51 or 0.31 m^3/s. The veloc-

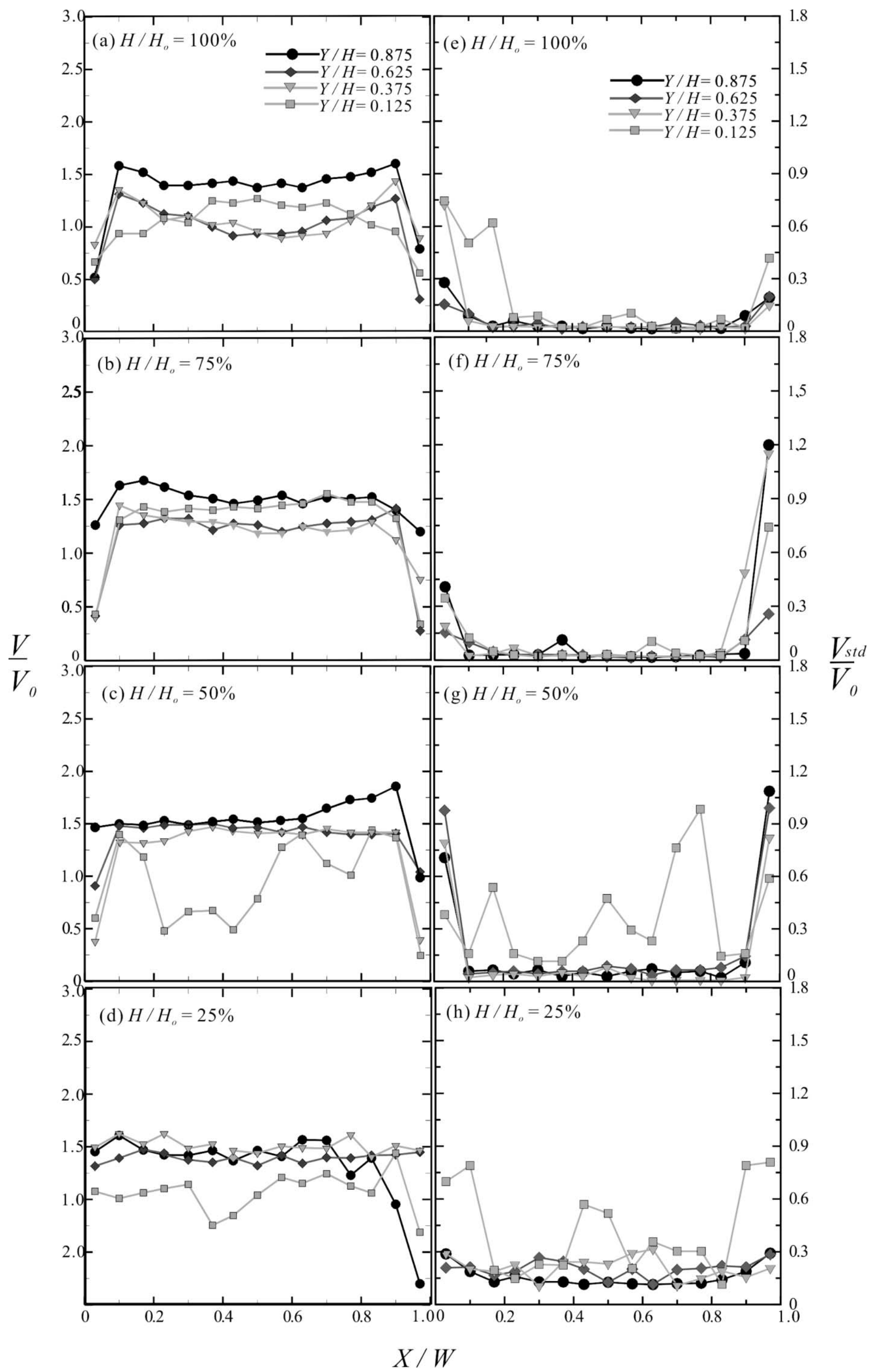

Fig. 6. Characteristics of face velocity distributions at Q = 0.51 m³/s. (a–d) dimensionless mean velocity, (e–h) dimensionless standard deviation of velocity fluctuation.

ity fluctuations near the side posts and doorsill are particularly larger than those in the core region. These regions with large turbulent fluctuations correspond to the locations of shear layers which are induced by the boundary layer separation as shown in Figs. 4 and 5.

Tracer gas test

Table 1 shows the results of the tracer gas experiments using the EN 14175-3 method. The sash height is set at H = 50 cm as prescribed by the method. Since the velocity characteristics discussed in the previous section show similar behaviors for different sash heights, the featured

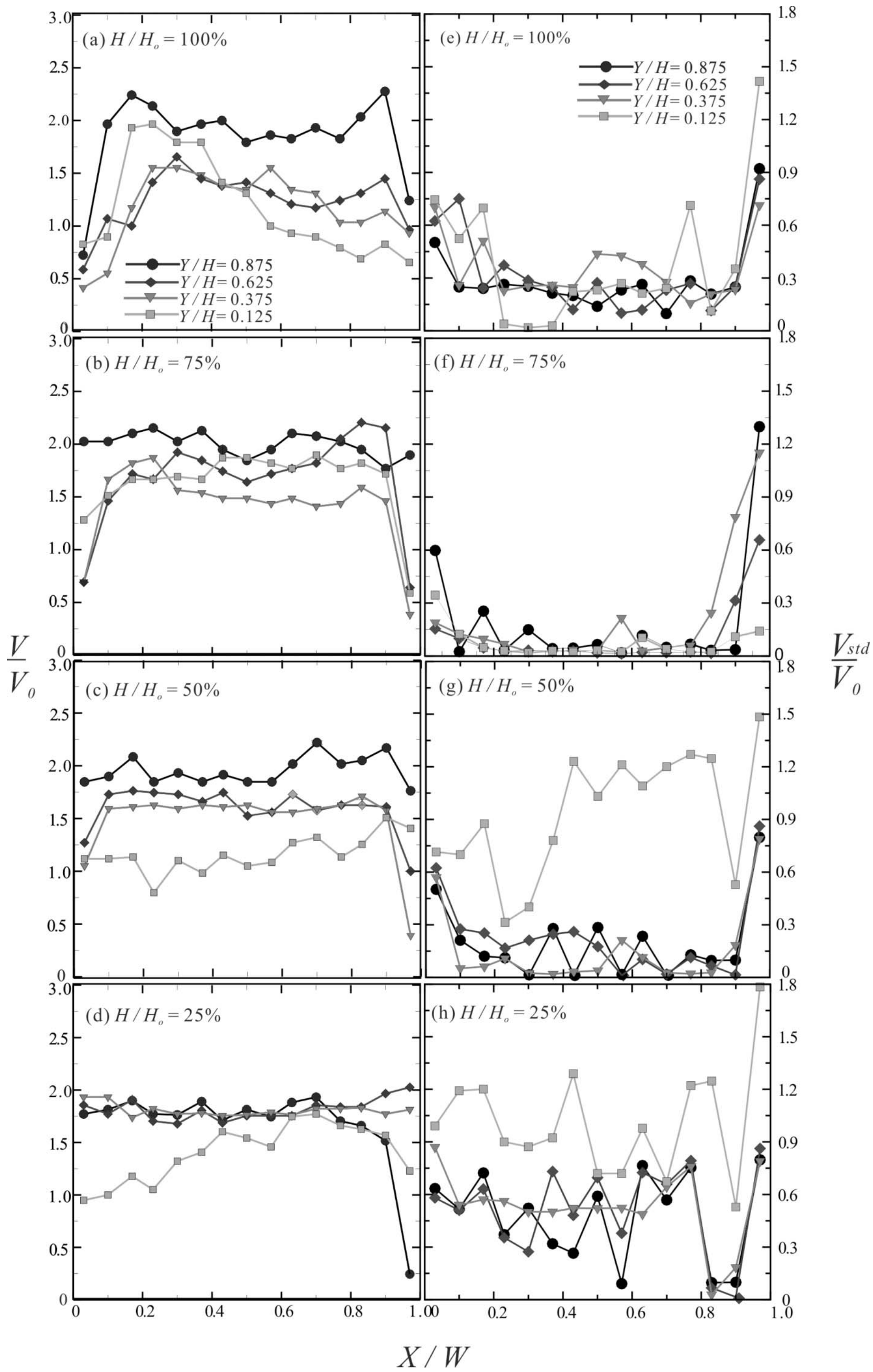

Fig. 7. Characteristics of face velocity distributions at Q = 0.31 m^3/s. (a–d) dimensionless mean velocity, (e–h) dimensionless standard deviation of velocity fluctuation.

results of the tracer gas concentration measurements at the prescribed sash height of 50 cm could be applied to discuss the correlations between the leakage and the flow at the other sash heights. At Q = 0.51 m^3/s, the level of SF_6 leakages measured at the upper grids, i.e., the grids P4, P5, and P6, are quite low (0.02–0.05 ppm). However, substantially high SF_6 concentrations (23.96–30.53 ppm) are detected at the grids P1, P2 and P3, i.e. at the right/left side and bottom edge of the hood opening. At Q = 0.31 m^3/s, the level of SF_6 leakages measured at the upper grids, i.e., the grids P4, P5, and P6, are quite low (0.07–0.24 ppm). With the same trend, significantly high

Table 1. Results of SF_6 tracer-gas concentration measurements of transparent prototype fume hood

Grid position	V_0 = 0.5 m/s	V_0 = 0.3 m/s
	$C_{SF6,ave}$ ($C_{SF6,peak}$) (ppm)	
P1	23.96 (47.14)	59.31 (75.99)
P2	27.37 (52.62)	51.76 (79.70)
P3	30.53 (44.60)	43.02 (67.13)
P4	0.02 (0.064)	0.08 (0.28)
P5	0.05 (0.073)	0.24 (0.87)
P6	0.02 (0.048)	0.07 (0.23)

Table 2. Results of SF_6 tracer-gas concentration measurements of commercial fume hoods

Fume hood	V_0 (m/s)	$C_{SF6,ave}$ ($C_{SF6,peak}$) (ppm)
#1	0.40	3.24 (14.52) @ bottom-right edge
#2	0.50	20.36 (58.29) @ bottom-middle edge
#3	0.32	67.87 (121.53) @ bottom-middle edge
#4	0.33	9.63 (31.14) @ bottom-middle edge
#5	0.44	77.90 (164.21) @ bottom-middle edge
#6	0.76	81.01 (210.75) @ bottom-middle edge
#7	0.44	2.87 (7.36) @ bottom-right corner
#8	0.46	5.66 (20.89) @ bottom-middle edge
#9	0.45	9.68 (22.20) @ bottom-middle edge
#10	0.56	0.98 (1.74) @ bottom-left corner
#11	0.30	101.54 (238.07) @bottom-middle edge

SF_6 concentrations (43.02–59.31 ppm) are detected at the grids P1, P2 and P3, i.e. at the right/left side and bottom edge of the hood opening. The peak values at P1, P2, and P3 present drastically large variations (44.6–52.62 ppm for Q = 0.51 m^3/s and 67.13–59.31 ppm for Q = 0.31 m^3/s) detected during the measurement periods. The peak values actually are indices of the leakage level variations. The dramatically large peak values apparently are induced by the large velocity fluctuations near the doorsill and side posts.

The results of the face velocity and velocity fluctuation measurements as well as the flow visualization show that the large-scale vortex structures occurring near the perimeter (particularly the doorsill and side posts) of the hood aperture could induce strong turbulence because of the boundary-layer separation. The recirculating vortical flows would entrain and carry the hood containments out of the hood aperture. Although the hood containments look like to be enclosed inside the vortical flow structure in the flow visualization pictures, the high turbulence fluctuations induced by the boundary-layer separation would enhance the momentum and mass exchanges across the separated boundary layer via the mechanism of turbulent dispersion. The crisis of containment leakage therefore is raised. The tracer gas experiment detects high degree of containment leakage around the perimeter of the hood aperture, which confirms the inference of flow visualization and velocity measurement. These results therefore establish the fact that the large-scale vortex structures occurring around the perimeters of hood aperture are due to the boundary-layer separation, which could induce strong turbulence, and therefore enhance dispersion of the hood containment.

Verification of commercial fume hoods

Table 2 shows the results of tracer gas concentration leakage tests on 11 commercial fume hoods. They are randomly selected among 9 universities in Taiwan. The hoods are operated at the face velocities set by the manufacturers. Leakage concentrations of SF_6 at all locations in the sash plane are measured. Only the maximum leakage concentrations and the locations where they are detected are listed in the Table. These face velocities are tuned by the manufacturers to obtain optimal hood performance. All these hoods are claimed by the domestic and foreign manufacturers for fine-tuned aerodynamics. Special techniques, e.g., doorsill airfoil (or streamlined doorsill), by-pass air, specially designed baffles, VAV, etc., have been installed to these fume hoods. The results listed in Table 2 show that these commercial hoods, although are operated at recommended face velocity V_0 ranging from 0.30 to 0.76 m/s and are well tuned to fit the requirements of aerodynamics (as claimed by the manufacturers), have dramatic local average leakages $C_{SF6,ave}$ ranging from 2.87 ppm to 101.54 ppm. The peak values $C_{SF6,peak}$ are also tremendously large, from 1.74 ppm to 238.07 ppm. Flow visualization pictures of these commercial hoods around the side posts and doorsill (which are not shown here) show clear boundary-layer separations. The most serious containment leakages listed in Table 2 are always detected along the doorsill where the boundary-layer separations are observed. It may be because that modifying the hood design to exactly fulfill the requirements of aerodynamics across the whole operation range is difficult, even though the VAV technique is employed. A new design technique which is called the "air-curtain isolated hood" as reported by Huang *et al.*[18, 19] may be an alternative to circumvent these difficulties.

Conclusions

This study clearly demonstrated the importance of the face velocity fluctuation features in laboratory fume hood performance. The face velocity/fluctuation profile and the overall concentration trend of contaminants along the face of the fume hood were obtained experimentally. Flow visualization tests demonstrated detailed flow patterns in different regions of the fume hood to qualitatively support the experimental results. The turbulent flow field over the three-dimensional edge of the hood involves the complex interaction between turbulent boundary layers, shear layers and separated flow regions. Dramatic face velocity fluctuations in large-scale, dynamic and instantaneous turbulent flow, in the vicinity of the boundary of the hood, explain the mechanism of the transport behavior. This complex interaction can easily contribute to the spread of contaminant leakage. The commonly used chemical fume hoods present prominent weakness around the areas near the doorsill and side poles. The high-leakage-risk around these regions is induced by the inappropriate aerodynamic design. Flow separation and accompanied recirculation occurred around these high-risk regions are the primary causes lead to turbulent diffusion and thus the contaminant spillage. The complexity of the interaction of multiple variables involved in the complex flow structures during the dynamic processes inhibits development of a model to establish the relationship between the parameters and contaminant leakage.

Acknowledgements

This research was supported by the Ministry of Education of Taiwan, R.O.C. under grant number 0940081791.

References

1) Ivany RE, First, MW, Diberardinis LJ (1989) A new method for quantitative, in-use testing of laboratory fume hoods. Am Ind Hyg Assoc J **50**, 275–80.
2) Fletcher B, Johnson AE (1992a) Containment testing of fume hoods - I methods. Ann Occup Hyg **36**, 239–52.
3) Fletcher B, Johnson AE (1992b) Containment testing of fume hoods - II test room measurements. Ann Occup Hyg **36**, 395–405.
4) Saunders T (1993) Laboratory fume hoods: a user's manual, 56–81, John Wiley & Sons, New York.
5) Volin CE, Joao RV, Reiman JS, Party E, Gershey EL (1998) Fume hood performance: face velocity variability inconsistent air volume systems. Appl Occup Environ Hyg **13**, 656–62.
6) Maupins K, Hitchings DT (1998) Reducing employee exposure potential using the ANSI/ASHRAE 110 method of testing performance of laboratory fume hoods as a diagnostic tool. Am Ind Hyg Assoc J **59**, 133–8.
7) Ekberg LE, Melin J (2000) Required response time for variable air volume fume hood controller. Ann Occup Hyg **44**, 143–50.
8) Durst F, Pereira JC (1991) Experimental and numerical investigations of the performance of fume hoods. Build Environ **59**, 153–64.
9) Durst F, Pereira JC (1992) Numerical simulation and optimization of the aerodynamics flow field inside fume hoods. Journal of Wind Engineering and Industrial Aerodynamics **40**, 127–45.
10) Hu P, Ingham DB, Wen X (1996) Effect of the location of the exhaust duct, an exterior obstruction and handle on the air flow inside and around a fume hood. Ann Occup Hyg **40**, 127–44.
11) Hu P, Ingham DB, Wen X (1998) Effect of baffles and a louvered bypass on the airflow and the convective patterns of contaminant inside a fume hood. Am Ind Hyg Assoc J **59**, 303–12.
12) Nicholson GP, Clark RP, de Calcina-Goff ML (2000) Computational fluid dynamics as a method for assessing fume hood performance. Ann Occup Hyg **44**, 203–17.
13) Lan NS, Viswanathan S (2001) Numerical simulation of airflow around a variable volume/constant face velocity fume hood. Am Ind Hyg Assoc J **62**, 303–12.
14) Kirkpatrick AT, Reither R (1998) Numerical simulation of laboratory fume hood airflow performance. ASHRAE Trans **98**, 1–13.
15) Tennekes H, Lumley JL (1972) A first course in turbulence, 121–215, The MIT Press, Cambridge.
16) European Committee for Standardization (2003) Fume cupboards-parts 3: type test methods (EN 14175-3), European Committee for Standardization, Brussels.
17) Tritton DJ (1988) Physical fluid dynamics, 231–53, Oxford University Press, New York.
18) Huang RF, Wu YD, Chen HD, Chen C-C, Chen C-W, Chang C-P, Shih T-S (2007) Development and evaluation of air curtain fume cabinet with its considerations of aerodynamics. Ann Occupational Hyg **51**, 189–206.
19) Huang RF, Chen HD, Hung C-H (2007) Effects of walk-by and sash movement on aerodynamics and contaminant leakage of air curtain-isolated fume hood. Ind Health **45**, 804–16.